Temperature Reversible Transitions in Linear Polyethylene Studied by TMDSC and Time-Resolved, Temperature-Modulated WAXD/SAXS

Bart Goderis,*,†,‡ Harry Reynaers,† Rolf Scherrenberg,‡ Vincent B. F. Mathot,†,‡ and Michel H. J. Koch§

Laboratory of Macromolecular and Structural Chemistry, Catholic University of Leuven, Celestijnenlaan 200F, B-3001 Heverlee-Leuven, Belgium; DSM Research, P.O. Box 18, NL-6160MD Geleen, The Netherlands; and European Molecular Biology Laboratory, EMBL c/o DESY, Notkestrasse 85, D-22603 Hamburg, Germany

Received October 11, 2000; Revised Manuscript Received December 22, 2000

ABSTRACT: The morphological changes during the quasi-isothermal melt crystallization of a linear polyethylene sample at 126 °C were monitored by synchrotron WAXD and SAXS and compared to TMDSC data. A blocklike temperature-profile with an amplitude of 1 °C and a period of 2 min was applied. AFM at room temperature reveals lamellar crystals with lateral dimensions of several micrometers that are composed of grains with dimensions comparable to those based on WAXD peak width analysis. According to the X-ray data all reversible melting and crystallization phenomena, probed by TMDSC, take place at the fold surface of the lamellar crystallites. There are no reversible changes at the crystal grain boundaries nor at the lateral surfaces of the lamellae, i.e., the crystal growth faces. The crystal growth rate, however, is affected by the temperature modulation.

1. Introduction

There is growing evidence for temperature reversible melting and crystallization phenomena in semicrystalline polymers, based on temperature modulated differential scanning calorimetry[1] (TMDSC) experiments. The magnitude of the complex heat capacity (also referred to as the reversing heat capacity), $|c_p^*|$, measured by TMDSC under quasi-isothermal conditions often displays an excess heat capacity superimposed to the baseline heat capacity.[2−4] The magnitude of this excess heat capacity depends on the polymer studied, its thermal history and the absolute temperature around which the small temperature modulation takes place.[5] Reversible melting and crystallization implies crystallization without the need for supercooling and consequently falls out of the realm of classical polymer crystallization theories that rely on nucleation concepts.[6,7]

These reversible processes are believed to occur at an active surface of the lamellar crystallites, which, in principle, can be the lateral surface or the fold surface or both. Advocates of fold surface melting discard lateral surface melting because on a lateral surface the melting point depends on the thickness of the lamella. If a lamella (or part of it) melts along this route and if recrystallization follows during the cooling part of the temperature cycle, the lamella will become thicker and hence no longer susceptible to melting in a subsequent cycle.[5] This process is thus irreversible and should disappear upon long-time annealing. Only at very high temperatures near the (equilibrium) melting temperature of very thick lamellar crystals could the temperature excursions applied in a typical TMDSC experiment (that is usually below 1 °C) be sufficiently large to bridge the gap between melting and crystallization.[8]

* To whom correspondence should be addressed. E-mail: bart.goderis@chem.kuleuven.ac.be.
† Catholic University of Leuven.
‡ DSM Research.
§ European Molecular Biology Laboratory.

There is plenty of evidence for temperature reversible phenomena far below the equilibrium melting temperature of crystallizable polymers even after long-term annealing.[4,9−11] At least in the case of (linear) polyethylene there is also some independent evidence for fold surface melting and crystallization,[12−16] based on small-angle X-ray scattering (SAXS). Hitherto, reversibility has never been explored using SAXS in combination with the small temperature excursions characteristic of TMDSC. It has, however, been argued,[10] based on considerations of lamellar habits, that the small hysteresis of the temperature dependence of the crystallinity and the lamellar thickness, which is usually measured when large temperature differences are covered, is incompatible with the notion of true reversibility.

A reversible excess heat capacity also exists in the case of very imperfect polyethylene crystals grown from ethylene-1-octene random copolymers with a relatively high 1-octene content.[10] Such crystals have limited lateral dimensions and there is no reason for the origin of the excess signal to be identical to that associated with mature lamellar crystals. Ethylene copolymers with an even higher comonomer contents probably crystallize as fringed micelles and in the extreme case of a very high comonomer content only nearest-neighbor ethylene sequences crystallize at temperatures close to the glass transition temperature.[17−19] Such a "cluster crystallization" was visualized using Monte Carlo simulations by van Ruiten et al.,[20] and it is quite fascinating, although not unexpected, to observe small crystalline clusters appearing and disappearing with time at a given constant temperature. Low molar mass substances behave in a similar way at their equilibrium melting temperature. They crystallize without supercooling, and crystals and melt are equally probable. In principle, this type of equilibrium crystallization should give rise to a reversible excess heat capacity in a TMDSC experiment. Androsch and Wunderlich[10] see two possible locations for such a reversible (equilibrium) crystallization of chain segments in their ethylene

10.1021/ma001759y CCC: $20.00
Published on Web 02/10/2001

copolymer of lower 1-octene content. The first is found in chain segments that melt only partially because of their attachment to other, higher melting (lamellar) crystals, whereas the second one is found in secondary, fringed-micellar crystals, grown within the network of larger crystals. Extrapolation of this mechanism to LPE with lamellar crystals seems unjustified especially when the crystallinity is high and rather perfect lamellar crystals have grown at a high temperature.

The mechanism of reversible melting and crystallization is thus clearly not settled. The literature on the subject is rather speculative since the reversing excess heat capacity signal in TMDSC does not provide any direct information about the morphological or molecular aspects of interest. Hence, the behavior of semicrystalline polymers under temperature modulated conditions must be explored by independent, structure-sensitive techniques.

Wide-angle X-ray diffraction (WAXD) and small-angle X-ray scattering (SAXS) are, in principle, well suited for this purpose. WAXD measurements provide information on changes of the crystalline density, the crystalline fraction and the lateral dimensions of the crystals provided the crystals exceed a critical size.[19] SAXS data yield values for the crystalline and amorphous layer thickness, the specific inner surface and the local and overall crystallinity as a function of time and temperature. High brilliance synchrotron X-ray sources must, however, be used to collect data at short sampling intervals during the rather fast oscillating temperature programs typical for TMDSC experiments. A particularly careful data analysis is an essential prerequisite since the morphological effects are expected to be small.

The present paper reports the results of a (quasi-) isothermal crystallization of a linear polyethylene (LPE) from the melt at 126 °C during which a temperature modulation with an amplitude of 1 °C and a period of 2 min was applied. This process was monitored for 90 min using simultaneous synchrotron SAXS and WAXD and the results are compared with similar off-line TMDSC data. LPE was selected because it is known to exhibit a very pronounced excess heat capacity compared to other semicrystalline polymers. The situation studied here can be considered as an archetype for reversible melting and crystallization phenomena in fairly perfect lamellar crystals. Similar studies on other homopolymers and less-perfect, semicrystalline ethylene copolymers will be reported in subsequent papers.

2. Experimental Section

2.1. Material and Temperature Program. All measurements were performed on a linear polyethylene (DSM code: JW1114), synthesized using a single-site Vanadium-based catalyst,[21] with a weight-average molar mass of 52 300 g/mol and a polydispersity (M_w/M_n) of 3.2.

For the TMDSC experiment the sample was first heated to 200 °C to erase its thermal history. After 6 min, it was cooled to 126 °C at 5 °C/min and subsequently subjected to a sinusoidal temperature oscillation with an amplitude of 1 °C and a period of 60 s. For the SAXS/WAXD experiments the temperature was controlled by a Mettler FP-82HT hot stage, flushed with cooled air. The sample was first cooled from 200 to 127 °C at 10 °C/min. Subsequently a temperature modulation was started by connecting cycles that consist of a cooling ramp from 127 to 125 °C at 3 °C/min, an isothermal waiting time of 19.6 s, a heating ramp to 127 °C at 3 °C/min, and a waiting time of 19.6 s. This program corresponds to a blocklike temperature modulation around 126 °C with an amplitude of 1 °C and a period of 119.2 s, which is twice that of the TMDSC experiment. Consequently the crystallization kinetics may be a little slower in the TMDSC experiment because the residence time at low temperature is shorter. The excess signal measured by TMDSC no longer depends on the period once the main crystallization is over and provided the period is longer than 60 s.[5] Hence, the relatively short period used in TMDSC does not impede the comparison with the modulated SAXS−WAXD experiments nor does the exact shape of the temperature profile. The magnitude of the amplitude may be sufficiently large to have some influence on the crystallization kinetics,[4] but it is also sufficiently small not to cover the temperature gap between melting and (classical) crystallization involving nucleation.[5]

2.2. TMDSC. The TA Instruments heat flux DSC 2920 was equipped with a refrigerated cooling system and purged with helium (25 mL/min). The temperature was calibrated using cyclohexane and indium, which was also used for enthalpy calibration. The heat capacity (c_p) was calibrated to the expected value for amorphous PE at 126 °C (c_{p_a} = 2.496 J/(g·°C)[22]) using the $|c_p^*|$ data at times shorter than 5 min in the quasi-isothermal measurement of interest. Perforated aluminum pans (Perkin-Elmer, 50μL) were used throughout, and the LPE mass was 4.685 mg. Scherrenberg et al.[4] introduced the nomenclature adopted here.

$|c_p^*|$ was calculated from the amplitude of the heat-flow, A_{Φ_ω}, the frequency of the temperature modulation, ω (=$2\pi/p$, with p the period) and the amplitude of the temperature modulation, A_T, according to

$$|c_p^*| = \frac{A_{\Phi_\omega}}{\omega A_T} K \tag{1}$$

K being a calibration constant. The crystallinity as a function of time, $w_c(t)$, was calculated by dividing the partial integral of the smoothed heat flow signal by, Δh, the reference transition enthalpy of PE at 126 °C (293.22 J/g).[22] Finally, using these $w_c(t)$ values, the baseline heat capacity, c_{p_b}, was calculated

$$c_{p_b} = w_c(t)c_{p_c} + (1 - w_c(t))c_{p_a} \tag{2}$$

with c_{p_c} and c_{p_a} the reference c_p values of respectively crystalline (c_{p_c} = 2.419 J/(g·°C))[22] and amorphous PE at 126 °C. The excess heat capacity, c_{p_e}, due to reversible melting and crystallization was calculated from the difference, $|c_p^*| - c_{p_b}$, and was further related to the fraction of material that reversibly follows the temperature modulation, Δw_r using the relation

$$\Delta w_r = -\frac{2A_T\, c_{p_e}}{\Delta h} \tag{3}$$

The ratio $\Delta w_r/w_c(t)$ was calculated for comparison with the scattering data.

2.3. SAXS/WAXD. Time-resolved X-ray scattering experiments were carried out on the X33 double focusing camera of the EMBL in HASYLAB, on the storage ring DORIS of the Deutches Elektronen Synchrotron (DESY) at a wavelength of 1.5 Å.[23] The standard data acquisition system[24] was used with two delay line detectors connected in series.[25] For the WAXD, the orthorhombic 110 and 200 reflections of LPE (JW1114) quenched from the melt into liquid nitrogen were used for calibration of the 2θ-axis.[15] The scattering vector s (with s = 2(sin θ)/λ, 2θ the scattering angle and λ the wavelength) in the SAXS region was calibrated using the first nine orders of dry calcified collagen. Figure 1 illustrates the assembly of the LPE sample holder that was inserted into the Mettler hot stage.

Sets of subsequent frames of 20 s were recorded, corresponding to six frames per temperature cycle. One frame consisted of 6 s acquisition time and 14 s waiting time. Excessive irradiation was avoided by closing a mini-shutter placed upstream from the sample during the waiting periods. The time corresponding to a given data point was set to three seconds, which is in the center of the acquisition period. Data

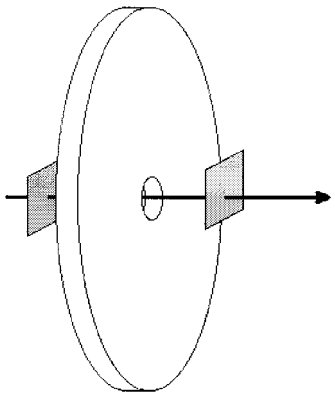

Figure 1. Schematic of the sample holder used for the SAXS/WAXD measurements. The perforated 1 mm thick brass disk with a diameter of 2 cm was placed in the Mettler hot stage. The sample is inserted by compression molding in the central hole, which has a diameter of 0.5 cm and is sealed on both sides with 15 μm thick aluminum foils (gray squares) that are fixed to the brass disk using temperature resistant tape (not shown). The arrow represents the X-ray beam.

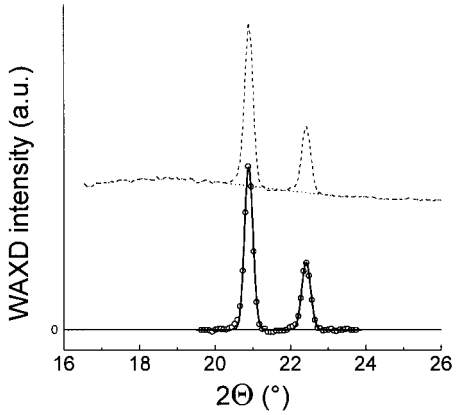

Figure 2. Top: Experimental WAXD data after 90 min pseudo-isothermal crystallization (dashed line) and baseline (dotted line) subtracted from the 110 and 200 reflections. The curves have been shifted along the ordinate axis for better visualization. Bottom: Result of subtraction (open circles) and fit by two Gaussians (full line).

were not recorded during the entire 90 min of the isothermal crystallization experiment but data collection was restricted to six segments between which the minishutter was closed. This, together with 14 s of shutter closing time per frame, reduced the total beam exposure to 14 min. The WAXD and SAXS intensities were normalized to the intensity of the primary X-ray beam and corrected for the response of the detectors.

WAXD data were collected in the range $16.5° < 2\theta < 37°$, and only the strong orthorhombic 110 and 200 reflections were used for analysis. They were stripped from the amorphous halo using straight lines before fitting with Gaussians as illustrated in Figure 2. A full decomposition, involving the determination of the amorphous halo was not attempted because of the limited angular range toward low angles. The sum of integrated intensities of the Gaussians (normalized to 1 at 90 min) was taken as a crystallinity index. The crystalline density was calculated from the angular positions of the Gaussian's maxima and accepting a constant length of 2.547 Å for the *c*-axis of the orthorhombic unit cell (the molecular chain direction). Finally, a (minimum)[26] crystallite size, D_{hkl}, in the direction perpendicular to the reflecting (*hkl*) planes was calculated using the Scherrer equation[27]

$$D_{hkl} = \frac{\lambda}{\beta_0 \cos\theta} \tag{4}$$

with β_0 the width at half-maximum (in radians) of the corresponding Gaussian.

An average melt pattern was subtracted from the SAXS patterns as a background,[15] yielding patterns denoted as $I(s)$. The range of data collection ($s < 0.032$ Å^{-1}) is in principle too short for an accurate Porod-type analysis.[15] In the present case, it is, however, sufficient since it has been shown earlier that the tail region of the SAXS pattern of a quenched LPE JW1114 strictly obeys Porod's law indicating the absence of transition layers between crystalline and amorphous regions and the absence of crystal edge effects.[15] It is shown below by AFM that the morphology after the quasi-isothermal crystallization applied here can also be modeled as an assembly of stacks of alternating crystalline and amorphous layers. With the two morphological constraints mentioned above the Porod constant, P, and the constant background due to density fluctuations within the individual phases, B, was determined accurately using the additional constraint that the integral of the interference function, IFF(s), equals zero,[28] that is

$$\int_0^\infty IFF(s)\, \mathrm{d}s = \int_0^\infty ((I(s) - B)s^4 - P)\, \mathrm{d}s = 0 \tag{5}$$

In practice the constants P and B were determined by linear regression of a Porod plot ($I(s)s^4$ vs s^4). The slope yields B, and the intercept equals P. Prior to the regression, equidistant data points were defined in the plot by interpolation in order to have an equal weight over the entire s^4 range. Using this procedure the B and P values are obtained that fulfill the condition expressed in eq 5. Interface distribution functions,[29] IDF(x), were calculated by Fourier transformation of the IFF(s) according to

$$\mathrm{IDF}(x) = -\int_0^\infty \mathrm{IFF}(s) \cos(2\pi x s)\, \mathrm{d}s \tag{6}$$

This integration was performed up to a sufficiently high s value (typically $s = 0.0125$ Å^{-1}), where IFF(s) has damped out to zero.[29] Note that IDF(0) = 0 only with the condition expressed in eq 5. Correlation functions, CF(x), were calculated by Fourier transformation of $[I(s) - B]$.

$$\mathrm{CF}(x) = \frac{\int_0^\infty [I(s) - B]s^2 \cos(2\pi x s)\, \mathrm{d}s}{Q} \tag{7}$$

Before transformation, $[I(s) - B]$ was extrapolated from the s value where the corresponding IFF(s) has reached zero to $s = 0.09$ Å^{-1} using a Porod-type function:[15]

$$\lim_{s\to\infty} (I(s) - B) = \frac{P}{s^4} \tag{8}$$

In eq 7, Q, represents the total scattering power, often referred to as the invariant, which for ideal two-phase structures (i.e., structures without any transition layers between the phases) can be written as[15]

$$Q = \int_0^\infty [I(s) - B]s^2\, \mathrm{d}s = C\alpha_S\phi_L(1-\phi_L)(d_c - d_a)^2 \tag{9}$$

with C a constant, α_S the volume fraction of semicrystalline regions, ϕ_L the (local) volume fraction crystallinity in the semicrystalline regions, and d_c and d_a the mass densities of the crystalline and amorphous phase, respectively. Theoretically, electron densities should be used in eq 9, but as only PE is present, it is correct to use mass densities provided a scale factor is included in the constant C.

2.4. AFM. Atomic force microscopy (AFM) experiments were performed with a Nanoscope IIIa scanning probe microscope equipped with a J-scanner. AFM images were obtained under ambient conditions while operating the instrument in the tapping mode and using a commercial Si-cantilever. Height and phase images were recorded simultaneously at the fundamental resonance frequency of the Si-cantilever (typically

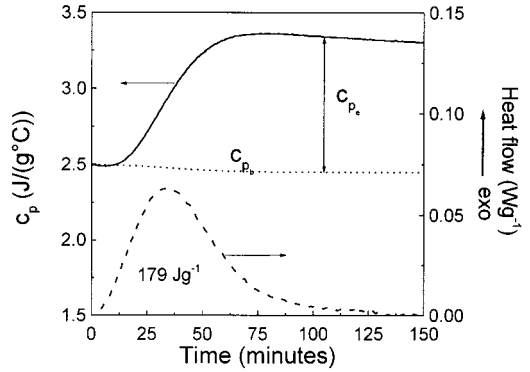

Figure 3. Illustration of the TMDSC-based $|c_p^*|$ (full line), c_{p_b} (dotted line), and (smoothed) heat flow (dashed line). c_{p_e} can be read from the difference between $|c_p^*|$ and c_{p_b}.

299−364 kHz) and with the tip−sample force interactions minimized. When operating in this "light-tapping regime" the height image shows the sample topography and topographic features are emphasized in the phase image.[30,31] Images were recorded with typical scan speeds of 0.5 lines/s. An LPE sample was prepared by 150 min quasi-isothermal crystallization as described above in the TA Instruments heat flux DSC 2920 followed by cooling to room temperature. The sample was taken out of the DSC pan and its surface was investigated without further treatment (i.e., no sectioning).

3. Results and Discussion

Figure 3 illustrates the (smoothed) total heat flow, c_{p_b} and c_{p_e} extracted from the TMDSC experiment. The increase of c_{p_e} qualitatively follows that of $w_c(t)$, represented by the full line in Figure 4, pointing to a proportionality between c_{p_e} and the amount of crystals. The ratio $\Delta w_r/w_c(t)$ beyond 80 min is fairly constant and close to 0.01. At shorter times, it is of the same order of magnitude but seems to be proportional to the overall crystallization rate with a maximum of 0.013 at the highest rate. A quantitative analysis of this phenomenon would, however, be very difficult since the overall (irreversible) change of the crystallinity during a temperature cycle is not negligible.[4]

To arrive at an estimate for the oscillation amplitude in the 80−90 min time window of the WAXD crystallinity index (see Figure 4) a Marquardt−Levenberg curve-fitting algorithm[32] was used with a three-parameter (P_1, P_2 and P_3) sinusoidal function

$$y = P_1 \sin(\pi(x + 79.95)) + P_2 + P_3 x \qquad (10)$$

P_1 being the amplitude of the oscillation. The period is fixed at 2 and the x-shift at 79.95. These values were obtained from a similar fit to the temperature profile, leaving the period and x-shift as free parameters, but with P_2 and P_3 fixed at 126 and 0 respectively.[33] The latter parameters account for the overall change of the fitted quantity. The WAXD crystallinity index increases more rapidly with time than the TMDSC-based crystallinity, most probably due to the slightly different temperature programs.

The amplitude of the oscillation in the WAXD crystallinity index in the 80−90 min segment equals 0.011 ± 0.002, based on a fit with eq 10, and is out of phase with the temperature modulation (insert in Figure 4). This corresponds to a WAXD-based $\Delta w_r/w_c(t)$ estimate of 0.021 ± 0.004, which is of the same order of magnitude although higher than the TMDSC value. The higher WAXD estimate may partially be due to the increase of

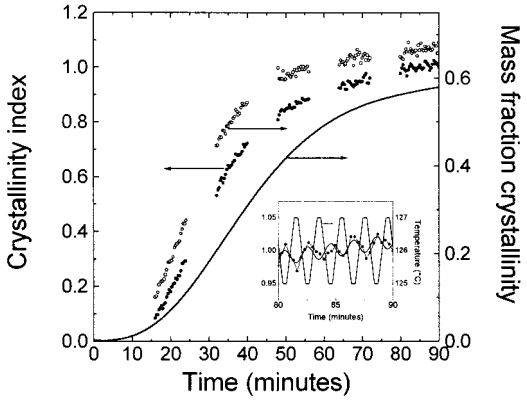

Figure 4. TMDSC (full line) and SAXS (open circles) overall mass fraction crystallinities and (normalized) WAXD crystallinity index (full circles) during quasi-isothermal crystallization. In the insert: the temperature profile (right-hand axis) and fit to the WAXD crystallinity index using eq 10 (full line).

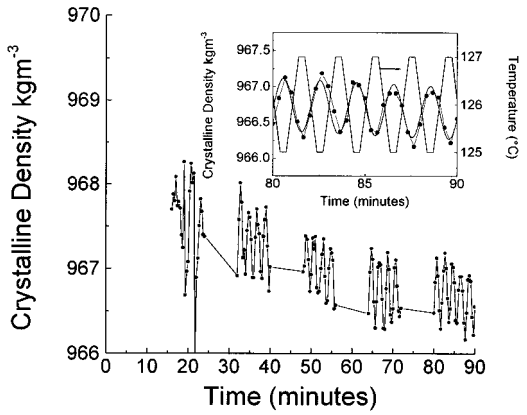

Figure 5. Evolution of the WAXD crystalline density of LPE during quasi-isothermal crystallization (full circles). The events in the 80−90 min segment are highlighted in the insert, which also includes the block like temperature profile (right-hand axis) and a fit to the data using eq 10 (full line).

thermal motion with increasing temperature. This diminishes the elastic Bragg intensity and introduces some inelastic thermal diffuse scattering.[34] Hence, both a decrease in crystallinity and an increase of the thermal motion tend to lower the intensity of the isolated Bragg reflections with increasing temperature and vice versa. The overall effect in this narrow temperature range is, however, too large to be solely due to changes in thermal motion. A change of temperature also affects the samples thickness and absorption. At constant crystallinity the associated relative change was calculated to be only 0.0005, which is negligible. The present WAXD data thus provide TMDSC-independent proof for reversible melting and crystallization in polymers. Unfortunately, the oscillation is too small to rise above the statistical fluctuations at times shorter than 80 min.

In Figure 5 the WAXD-based crystalline density is represented, which clearly oscillates out of phase with the temperature perturbation. The amplitude of this oscillation, obtained from a fit to the data in the 80−90 min segment using eq 10 (see insert in Figure 5), equals 0.36, which is close to the value of 0.35, predicted by Swan.[35] The density decreases slightly with time, which is not as expected, since crystallites should become more perfect and hence more dense upon annealing. Astonishingly, there seems to be no data in the literature concerning density changes during the initial state of

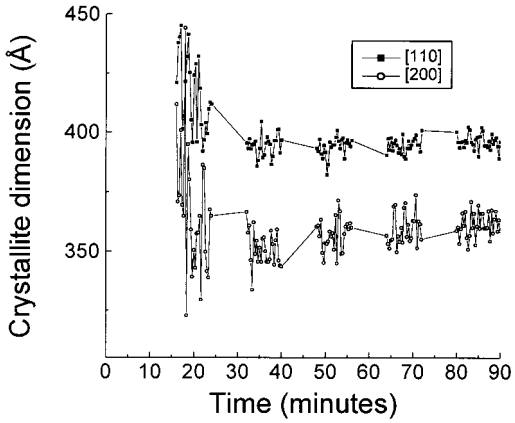

Figure 6. Estimates, based on a Scherrer type WAXD peak width analysis, for the (lateral) dimension of the crystal in a direction perpendicular to respectively the 110 and 200 reflecting planes.

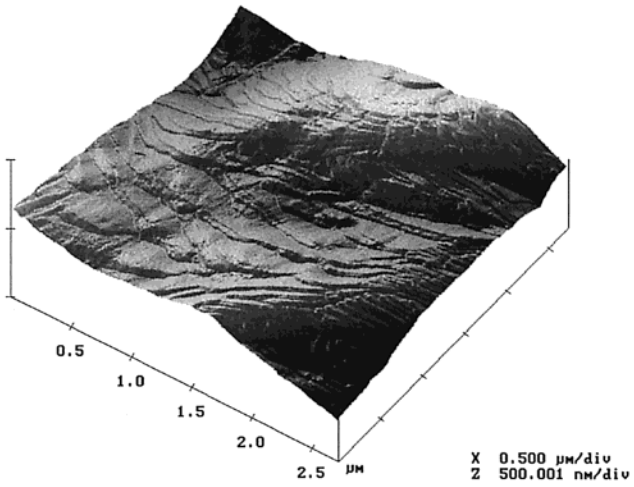

Figure 7. Illuminated side view of an AFM height image, illustrating the lamellar stack morphology after quasi-isothermal crystallization of the LPE at 126 °C.

crystallization. The observed decrease may point to more perfect crystals being formed first. An overall increase in density may occur once all crystals are formed and after longer annealing times than studied here.

The WAXD-based estimates for the lateral dimensions of the crystals are illustrated in Figure 6. The statistical noise is quite pronounced, and hence a fit with eq 10 would be meaningless. No direct conclusions can thus be drawn at this stage about possible changes induced by the temperature modulation.

The WAXD-based lateral dimensions of the crystals do not change significantly with time and are too small to be compatible with laterally extended lamellae. In contrast, Figure 7 clearly shows the existence of such morphology. In this AFM height image the crystals appear as quite regularly stacked platelike structures with lateral dimensions of several μm. This WAXD−AFM discrepancy can be accounted for by assuming a mosaic substructure, consisting of coherently scattering entities with cross sections of about 400 Å.

The phase image in Figure 8, representing the fold surface of these crystals at much higher magnification, reveals grainlike entities similar to those observed earlier for a number of synthetic polymers using AFM.[36,37] In the present case, their size resembles that of the coherently scattering entities, pointing either to

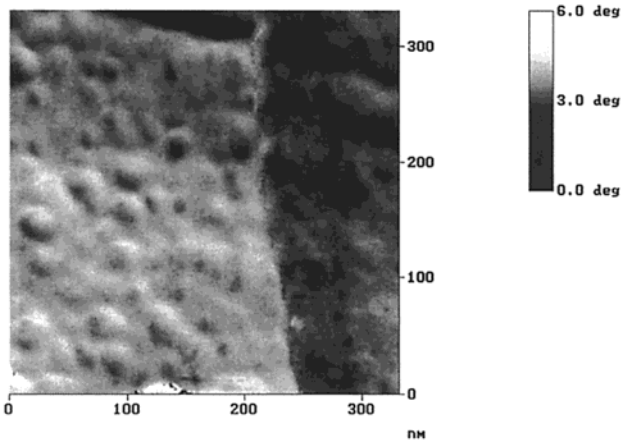

Figure 8. Tapping mode AFM phase image at high magnification of the LPE crystal fold surface after quasi-isothermal crystallization from the melt at 126 °C, illustrating the presence of small building blocks with a size comparable to that estimated from a Scherrer peak width analysis of the WAXD data.

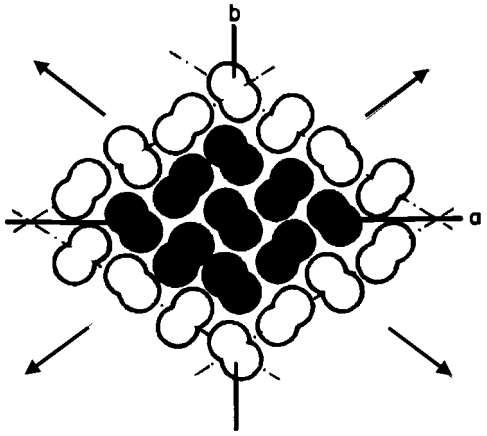

Figure 9. Central area of a lozenge shaped PE crystal (projection of the planar zizag chains on the *ab* plane). Growth of such a crystal is assumed to proceed in the direction of the arrows by addition of rows with adjacent folds along the 110 planes. The outer rows are filled in white in this image.

a progression of the crystalline substructure into the amorphous fold-surface layer or to the tapping being sufficiently hard to probe crystalline features through the amorphous layer.

At this point, the existence of active lateral surfaces can be discussed. The most central part (the nucleus) of a simple lozenge-shaped crystal with 110 growth faces is depicted in Figure 9.[38] Such a crystal may grow according to the arrows by addition of rows consisting of regularly folded PE, as observed after crystallization from solution.

In general, the morphology may be more complicated after crystallization from the melt; i.e., growth may occur along other crystallographic planes and possibly there is twinning.[38] Taking such a simplified 240 Å thick crystal (see SAXS results below) with 1 or 2 μm long edges as a model one finds that, to have a $\Delta w_r/w_c(t)$ of 0.0213, a melting of, respectively, 12 or 24 rows is needed at all edges. This corresponds to an inward melting at all sides of, respectively, 55 or 105 Å, which is rather drastic. In contrast, for a granular building block with edges of about 400 Å an inward melting of less than one layer is sufficient since in this case an all-side-one-row inward melting already accounts for a

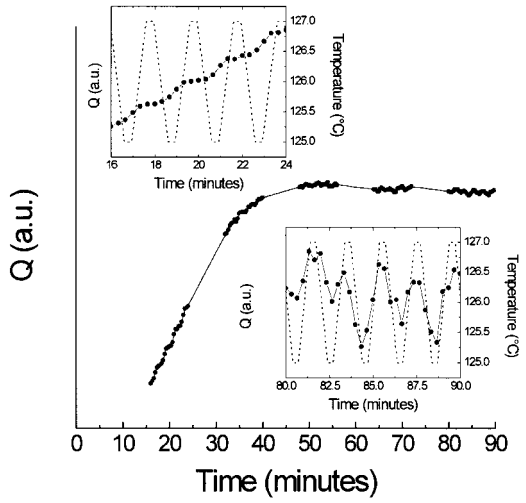

Figure 10. Total SAXS scattering power (Q) as a function of time (connected filled circles). The upper left insert magnifies the 16−24 min segment and highlights the relation with the temperature modulation (dashed line). The lower right insert is a similar magnification of the 80−90 min segment.

$\Delta w_r/w_c(t)$ of 0.046. For fold surface melting one can easily calculate that a 2.53 Å inward melting on both sides of a 240 Å thick lamellar crystal suffices to achieve a $\Delta w_r/w_c(t)$ of 0.0213. This corresponds approximately to a single PE unit cell in the chain direction (c-axis). On the basis of the present experimental results and calculations, two possible locations can thus be envisaged for temperature reversible melting and crystallization of LPE lamellar crystals: inside the crystals (possibly at the crystal grain boundaries) or at the crystal fold surface. SAXS can distinguish between these as discussed below.

Figure 10 illustrates the initial sharp increase of the total SAXS scattering power, Q, which changes into a slight decrease after 50 min. The superimposed oscillation represents the direct response of Q to the temperature perturbation and has time dependent characteristics; i.e., the slope of Q in the 16−24 min segment is lower at high temperatures but never becomes negative (upper left insert in Figure 10) whereas Q clearly oscillates in phase with temperature in the 80−90 min segment (lower right insert in Figure 10).

According to eq 9 Q depends on four variables and on the constant C. The obvious in-phase oscillation of Q with temperature because of the temperature dependence of the density factor $(d_c - d_a)^2$ has a negligible contribution to the observed amplitude of the Q oscillation.[35] Consequently, the response of Q to the temperature perturbation must be related to changes of the amorphous−crystalline volume fractions (involving α_S or ϕ_L or both) or changes of d_c not caused by thermal expansion. The latter refers to the option of having active crystal grain boundaries. Such reversible melting and crystallization would give rise to a decrease and increase of d_c respectively,[39] which in combination with a (nearly) constant d_a would result in an oscillation of $(d_c - d_a)^2$, and hence of Q, that is out of phase with that of the temperature. This hypothesis can be discarded because an in-phase oscillation is actually observed in the 80−90 min segment (the evolution of Q in some earlier segments is different, which will be addressed at the end of this "Results and Discussion" section). The alternative of having active lateral surfaces may influence both α_S and ϕ_L, whereas fold surface melting would

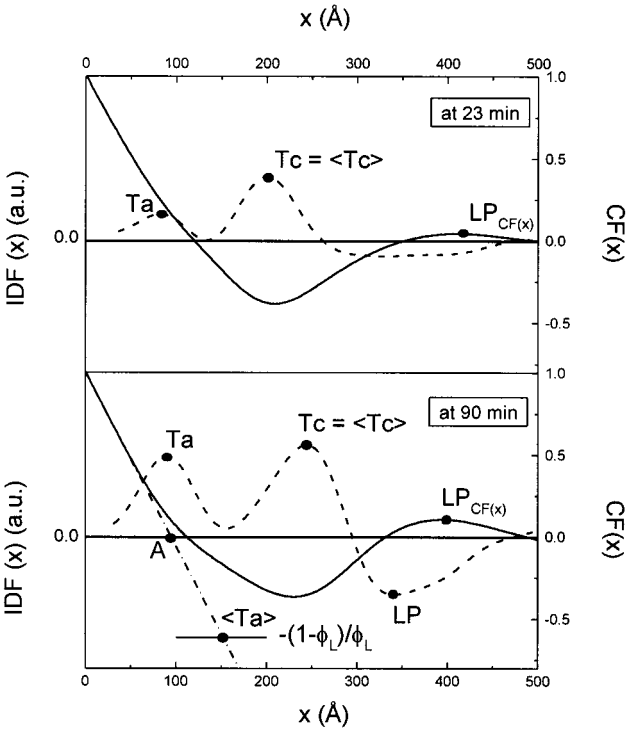

Figure 11. Extraction of the morphological parameters from interface distribution functions, IDF(x) (dashed lines) and correlation functions, CF(x) (full lines). The dash−dot line in the 90 min part represents a linear regression to the autocorrelation triangle of CF(x) which intersects the abscissa at A and the horizontal full line at $-(1 - \phi_L)/\phi_L$ yielding $\langle T_a \rangle$, the average size of the amorphous layer thickness.

only affect ϕ_L. In the former case, the lateral dimensions of the semicrystalline regions may decrease or increase in favor of or at the expense of surrounding amorphous material, which directly would act upon α_S. This option is, however, also unrealistic since it would result in an out-of-phase oscillation of Q. Hence, only the factor $\phi_L(1 - \phi_L)$ can be responsible for the oscillation of Q in-phase with temperature and out-of-phase with the crystallinity, implying that ϕ_L has to be larger than 0.5. In the case of active lateral surfaces the periodic increase or decrease of ϕ_L should go together with a decrease or increase of the number-average long period, $\langle LP \rangle$, due to the insertion or removal of lamellar parts between existing crystalline layers. For fold surface activity the crystalline lamellar thickness should decrease or increase at the expense of the amorphous layer thickness without significantly affecting the long period. The shape of the SAXS patterns has to be investigated to discriminate between both, which is most easily done by considering the Fourier transforms, CF(x) and IDF(x).

In Figure 11 two sets of IDF(x) and CF(x) functions, corresponding to 23 and 90 min respectively, are displayed. The first two positive peaks in IDF(x) represent the thickness distribution of the amorphous and crystalline layer respectively, whereas the first negative contribution at higher x is related to the thickness distribution of the long period.[29] The maxima in these distributions, which can be considered as most probable values, are labeled T_a, T_c, and LP, respectively. For the curve at 23 min, no LP could be assigned because the long period distribution is too broad.

According to Babinet's principle, it is impossible to decide without additional information which distribution corresponds to the amorphous or crystalline layer

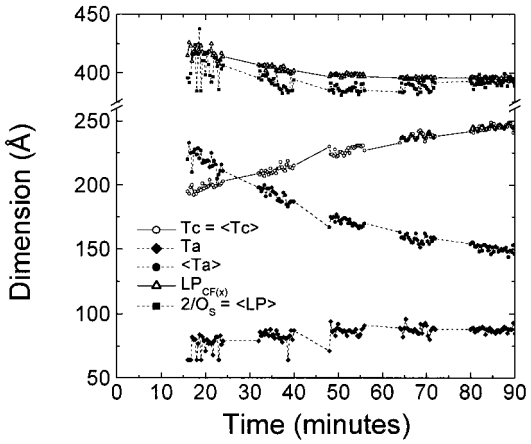

Figure 12. Morphological parameters as a function of time, as explained in the legend, based on a lamellar stack model and extracted from the IDF(x) and CF(x) functions. The thick, oscillating full line through the 64−72 min T_c data is a fit using eq 10 (see also Figure 13). The similar line through the 80−90 min T_c data is not a fit through the displayed IDF(x)-based values but represents a fit through the corresponding Q_a-based T_c data for comparison (see also Figure 15).

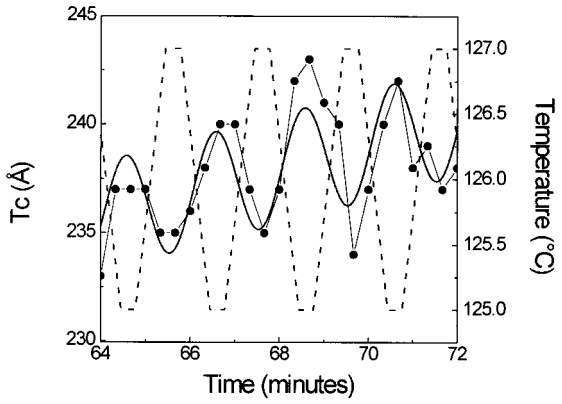

Figure 13. T_c as a function of time in the 64−72 min segment (full circles). The thick full line represent a fit through these data using eq 10 and the dashed line corresponds to the temperature profile of which the ordinate is on the right-hand side.

thickness. Here, the labeling is based on a previous isothermal (re)crystallization experiment at 125 °C on this particular LPE sample in which the crystalline layer thickness resembles that of the second thickness distribution in the present experiment.[16] This labeling is also compatible with a ϕ_L value larger than 0.5. The evolution of T_c and T_a with time is illustrated in Figure 12. T_c increases with time according to earlier observations,[16,40,41] whereas T_a remains almost constant.

In addition, the T_c values of the 64−72 min segment clearly display an oscillation out-of-phase with that of the temperature, which is enlarged and fitted with eq 10 in Figure 13. The amplitude of the fitted curve equals 2.5 ± 0.5 Å and coincides with the model calculation for fold surface melting (2.53 Å).

The oscillation of T_c in earlier segments is masked by noise since the corresponding scattering patterns from which the IDF(x) are derived, are less intense and hence less suitable for high accuracy evaluation. The (apparent) asymmetric crystalline layer thickness distribution at 90 min is indicative for an overlap of the crystalline layer thickness distribution with the (negative) contribution of the long period. Most likely the oscillation of T_c in the 80−90 min segment is less manifest because of this overlap. Although the data in Figure 13 provide direct evidence for reversible fold surface melting they do not exclude the possibility of concomitant activity at the lateral surfaces. This can be evaluated from the number-average long period, ⟨LP⟩, calculated below and which differs from the most probable value, LP. According to the model of laterally extended lamella ϕ_L can be written as $\langle T_c\rangle/\langle LP\rangle$, with $\langle T_c\rangle$ the number-average crystalline layer thickness. Judging from the IDF(x) in Figure 11, the crystalline thickness distribution looks fairly symmetrical aside from the overlap with the long period distribution of opposite sign. Consequently, T_c is considered equal to $\langle T_c\rangle$. Equation 11 was used to calculate ϕ_L and ⟨LP⟩, the latter being equal to $2/O_S$ in the case of laterally extended lamellae and with O_S the specific inner surface.[15]

$$A = \phi_L(1-\phi_L)\frac{2}{O_S} = \phi_L(1-\phi_L)\langle LP\rangle = (1-\phi_L)\langle T_c\rangle \tag{11}$$

The parameters A and $\langle T_c\rangle$ were used as input, A being the intersection of the linear regression to the autocorrelation triangle (LRAT) of CF(x) with the abscissa.[15] The location of A is illustrated in Figure 11, and the evolution of ⟨LP⟩ with time is depicted in Figure 12. The latter data decrease asymptotically to a fairly constant value beyond 60 min. Unfortunately, due to noise, it is not possible to decide whether these data are truly constant or whether a small oscillation is superimposed. The data closely resemble the $LP_{CF(x)}$ data in Figure 12, which are long period estimates based on the first side maximum in CF(x) (see also Figure 11). Whether or not $LP_{CF(x)}$ approximates ⟨LP⟩ depends on the applicability of the one-dimensional lamellar stack model and on the actual stacking statistics.[42] The near match of these parameters in the present case—at least—supports the use of the model and justifies the postulate $T_c = \langle T_c\rangle$. In addition, the $LP_{CF(x)}$ values are sufficiently constant beyond 60 min to support the absence of lateral surface effects.

It is of interest to investigate whether an oscillation of T_c similar to that in the 64−72 min segment can cover the oscillation of Q in the 80−90 min segment where the oscillation of T_c is assumed to be hidden in IDF(x). To do so, Q was scaled to $\phi_L(1-\phi_L)$ in this particular segment using the average ratio between Q and $\phi_L(1-\phi_L)$, after performing a (minor) correction for the thermal expansion related changes in $(d_c - d_a)^2$ and assuming space filling semicrystalline regions in this particular time segment (i.e., $\alpha_S = 1$).[15] By this procedure the Q values are made absolute since the scaling factor represents the constant C in eq 9. Note that for this evaluation ϕ_L was calculated from

$$\phi_L = \frac{\langle T_c\rangle}{LP_{CF(x)}} \tag{12}$$

yielding ϕ_L data that are not as noisy as those based on eq 11. Finally, using these corrected and absolute Q values, denoted as Q_a, another set of ϕ_L data, denoted as $\phi_{L,Qa}$, was calculated by solving

$$Q_a = \phi_{L,Qa}(1-\phi_{L,Qa}) \tag{13}$$

The products $\langle LP\rangle\phi_{L,Qa}$ and $\langle LP\rangle(1-\phi_{L,Qa})$ are shown in Figure 14, representing $\langle T_c\rangle_{Qa}$ and $\langle T_a\rangle_{Qa}$ values,

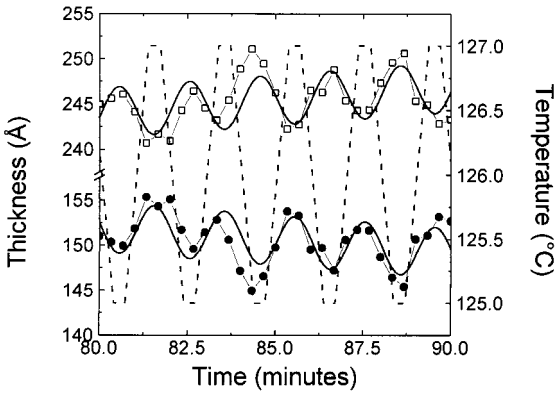

Figure 14. Q_a-based $\langle T_c \rangle$ (open squares) and $\langle T_a \rangle$ (full circles) values. The full lines are fits with eq 10 and the dashed line displays the temperature profile of which the ordinate is situated at the right-hand side. The fit through the $\langle T_c \rangle$ data is included in Figure 12 for comparison with the IDF(x)-based T_c data.

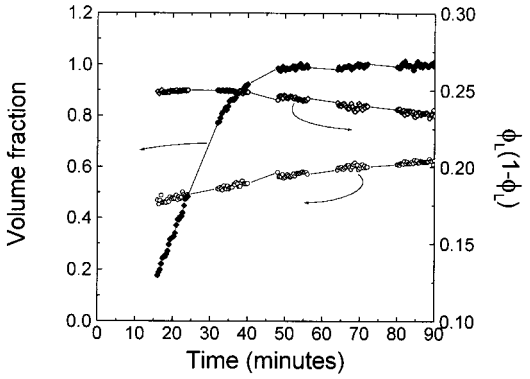

Figure 15. ϕ_L (open circles) and α_S (full squares): left-hand ordinate; $\phi_L(1 - \phi_L)$ (open diamonds): right-hand ordinate.

respectively. To avoid the introduction of extra noise a constant $\langle LP \rangle$ of 396 Å was used, which is the average of $LP_{CF(x)}$ in the 80−90 min segment.

The amplitude of $\langle T_a \rangle_{Qa}$ based on a fit with eq 10 equals 2.8 ± 0.5 Å, which—taking the error into account—equals previous estimates. Consequently, there are no arguments for active lateral surface activity on top of reversible fold surface melting since the observed T_c oscillation entirely covers the oscillation in Q, at least beyond 60 min. This statement, however, does not hold for the oscillations in earlier segments, which have different characteristics as pointed out in the discussion related to Figure 10. The contribution of α_S and ϕ_L to the evolution of Q is discussed below over the entire experiment. This involves the determination of α_S and the overall crystallinity $\alpha_S\phi_L$.

The ϕ_L data based on eq 11 are shown in Figure 15 together with the product $\phi_L(1 - \phi_L)$. Dividing Q_a by $\phi_L(1 - \phi_L)$ yields α_S, according to eq 9 and the definition of Q_a given above. The overall volume-fraction crystallinity, $\alpha_S\phi_L$, was transformed into mass-fraction crystallinity using Swan's density values for amorphous and crystalline PE.[35] This allows a direct comparison with the DSC- and WAXD-based mass-fraction estimates in Figure 4. The SAXS values are higher, in agreement with earlier work.[16] The qualitative evolution, however, is comparable, pointing to a consistent data evaluation. In the earliest segments α_S increases from 0 to 1 with a clear oscillation superimposed. At relatively long times α_S equals 1, except for some inevitable noise. In the two earliest time segments the product $\phi_L(1 - \phi_L)$ is not sensitive to possible oscillations in ϕ_L since ϕ_L is very close to 0.5. Consequently, the oscillations of Q (see Figure 10) in these segments are entirely due to the temperature response of α_S, elucidating the difference in behavior compared to that of later segments, which—in contrast—are caused by changes in ϕ_L. The stepwise increase of Q and hence of α_S in these segments reflects the temperature dependence of the crystal growth rate, i.e., at low temperature the rate (and hence the slope of Q) is high whereas at high temperature it is low. It is important to note that, in this case, no melting is observed during a heating step (i.e., no decrease of Q or α_S) implying that the crystals formed at a lower temperature are stable at least 2 °C above their crystallization temperature. This observation supports the view that the small temperature perturbations applied here cannot induce reversible melting and crystallization at the lateral surfaces (the growth faces) of lamellar crystals. The growth rate is affected but never becomes negative, which would imply melting. Reversible fold surface melting, however, cannot be excluded even at these early stages of crystallization. In principle, less noisy IDF(x)-based T_c data could shed a light on this matter.

Finally, some general remarks can be made on the process of isothermal crystallization irrespective of the temperature modulation. Apparently, lamellar stacks are generated immediately from the beginning with an internal crystallinity, ϕ_L, close to 0.5 (see Figure 15). The fraction of these stacks, α_S, increases to fill space completely after 50 min. Concomitantly, ϕ_L increases due a thickening of the crystallites (increase of $\langle T_c \rangle$ in Figure 12) and by the insertion of new lamellae between existing ones. Lamellar insertion is evidenced by a decrease of $\langle LP \rangle$ and $\langle T_a \rangle$, the latter being calculated from

$$\langle T_a \rangle = LP_{CF(x)} - \langle T_c \rangle \tag{14}$$

Figure 12 displays the evolution of $\langle T_a \rangle$, the number-average amorphous layer thickness, which differs significantly from T_a, the most probable thickness. The x-position of $\langle T_a \rangle$ is added in Figure 11 for comparison with T_a. The former corresponds to the intersection of the linear regression to the autocorrelation triangle (LRAT) with a line at $y = -(1 - \phi_L)/\phi_L$.[15,43,44] Such a difference is to be expected for skew or multimodal layer thickness distributions. In the present case a multimodal distribution is most likely since, first, the amorphous peak around 80 Å in the IDF(x) functions is not skew at all and, second, the area under the crystalline peak is larger than under the amorphous one, whereas theory predicts them to be identical.[29] The latter observation is taken as evidence for a hidden very broad second moment of the amorphous layer thickness distribution, which should be at higher distances than the mode around 80 Å because $\langle T_a \rangle$ is larger than T_a. This second mode can only be extracted from IDF(x) functions by fitting according to an appropriate stacking model, of which the details in the present case are unknown. The single broad long period thickness distribution, however, points to a fairly random alternation of the crystalline layers with amorphous ones of variable thickness. The area under the amorphous peak around 80 Å increases with time whereas its maximum (T_a) remains constant. This supports the existence of a (temperature dependent) characteristic amorphous layer thickness as suggested by Strobl et al.[14] Accordingly,

the crystallinity in a stack only increases by the insertion of new crystalline lamellae between already existing ones, provided amorphous layers are generated that are not thinner than the mentioned characteristic one.[13] Consequently, the fraction of amorphous layers with the characteristic thickness is expected to increase at the expense of amorphous layers that are at least as thick as the sum of a crystalline layer and twice the characteristic amorphous layer thickness. The increasing area under the 80 Å peak in the amorphous layer thickness distribution with time, most likely at the expense of the (hidden) second moment in the amorphous thickness distribution, supports secondary crystallization along this line (see Figure 11).

4. Conclusions

The characteristics of temperature reversible phenomena in the case of a linear polyethylene sample during quasi-isothermal crystallization were studied using TMDSC, AFM and synchrotron WAXD/SAXS. TMDSC reveals reversible melting and crystallization, which is confirmed independently by WAXD and SAXS. The TMDSC estimate for the amount of the crystalline fraction taking part in this process is, however, only half that of the WAXD and SAXS estimates. The lower TMDSC value may be due to a lower transition enthalpy, Δh, associated with this reversible process (see eq 3) compared to that applicable to nonreversible melting; i.e., the transition from a crystalline orthorhombic phase to a random melt. The reversible process clearly is different in nature since it takes place at the lamellar fold surface according to the SAXS results. The lateral surfaces of the crystallites can be excluded as potential sites for reversible melting based on calculations, the constancy of the long period and on the nonreversible character of crystallization at the (lateral) growth faces. Moreover, fold surface melting entirely covers the reversible change of the SAXS invariant, leaving no space for concomitant lateral surface activity. There is no visible response to the temperature modulation of defects in the crystals that possibly are situated at the crystal grain boundaries. The grains in the lamellar crystals observed by AFM are tentatively associated with the coherently scattering entities of the lamellae since they have a size comparable to that estimated from a Scherrer peak width analysis of the WAXD data.

References and Notes

(1) Reading, M. *Trends Polym. Sci.* **1993**, *8*, 248.
(2) Okazaki, I.; Wunderlich, B. *Macromolecules* **1997**, *30*, 1758.
(3) Ishikiriyama, K.; Wunderlich, B. *Macromolecules* **1997**, *30*, 4126.
(4) Scherrenberg, R.; Mathot, V.; Steeman, P. *J. Therm. Anal.* **1998**, *54*, 477. Scherrenberg, R.; Mathot, V.; van Hemelrijck, A. *Thermochim. Acta* **1999**, *330*, 3.
(5) Hu, W.; Albrecht, T.; Strobl, G. *Macromolecules* **1999**, *32*, 7548.
(6) Hoffman, J. D. *Polymer* **1982**, *23*, 656. Hoffman, J. D. *Polymer* **1983**, *24*, 3.
(7) Wunderlich, B. Crystal Nucleation, Growth, Annealing. In *Macromolecular Physics*; Academic Press: New York, 1976; Vol. 2.
(8) Wunderlich, B.; Okazaki, I.; Ishikiriyama, K.; Boller, A. *Thermochim. Acta* **1998**, *324*, 77−85.
(9) Schick, C.; Merslyakov, M.; Wunderlich, B. *Polym. Bull.* **1998**, *40*, 297.
(10) Androsch, R.; Wunderlich, B. *Macromolecules* **1999**, *32*, 7238.
(11) Toda, A.; Oda, T.; Hikosaka, M.; Saryama, Y. *Polymer* **1997**, *38*, 231.
(12) Tanabe, Y.; Strobl, G. R.; Fisher, E. W. *Polymer* **1987**, *27*, 1147.
(13) Strobl, G. R.; Schneider, M. J.; Voigt-Martin, I. G. *J. Polym. Sci.: Polym. Phys. Ed.* **1980**, *18*, 1361.
(14) Albrecht, T.; Strobl, G. *Macromolecules* **1995**, *28*, 5827.
(15) Goderis, B.; Reynaers, H.; Koch, M. H. J.; Mathot *J. Polym. Sci.: Part B: Polym. Phys.* **1999**, *37*, 1715.
(16) Goderis, B.; Peeters, M.; Mathot, V. B. F.; Koch, M. H. J.; Bras, W.; Ryan, A. J.; Reynaers, H. *J. Polym. Sci.: Part B: Polym. Phys.* **2000**, *38*, 1975.
(17) Bensason, S.; Minick, J.; Moet, A.; Chum, S.; Hiltner, A.; Baer, E. J. *Polym. Sci.: Part B: Polym. Phys.* **1996**, *34*, 1301.
(18) Mathot, V. B. F.; Scherrenberg, R. L.; Pijpers, M. F. J.; Engelen, Y. M. T. In *New trends in polyolefin Science and Technology*; Hosoda, S., Ed.; Research Signpost: Trivandrom, India, 1996; p 71.
(19) Vanden Eynde, S.; Mathot, V.; Koch, M. H. J.; Reynaers, H. *Polymer* **2000**, *41*, 3437.
(20) van Ruiten, J.; van Dieren, F.; Mathot, V. B. F. In *Crystallization of Polymers*; Dosiére, M., Ed.; Kluwer Academic Publishers: Dordrecht, The Netherlands, 1993; p 481.
(21) Hunter, B. K.; Russell, K. E.; Scammell, M. V.; Thompson, S. L. *J. Polym. Sci., Polym. Chem. Ed.* **1984**, *22*, 1383.
(22) Mathot, V. B. F. *Polymer* **1984**, *25*, 579.
(23) Koch, M.; Bordas, J. *Nucl. Instrum. Methods* **1983**, *208*, 435.
(24) Boulin, C.; Kempf, R.; Gabriel, A.; Koch, M. *Nucl. Instrum. Methods* **1988**, *A269*, 312.
(25) Rapp, G.; Gabriel, A.; Dosière, M.; Koch, M. *Nucl. Instrum. Methods* **1995**, *A357*, 178.
(26) A "minimum" crystallite thickness refers to the fact that, besides a reduction of the crystallite size, microstrains and paracrystalline distortions also tend to broaden a Bragg reflection. These contributions can be separated provided higher order reflections are considered. Accordingly, underestimated crystallite sizes are obtained if the width of a single reflection is associated with crystallite size.
(27) Alexander L. E. In *X-ray Diffraction Methods in Polymer Science*; Robert, E., Ed.; Krieger Publishing Co.: Hunington, New York, 1979; p 423.
(28) Albrecht, T.; Strobl, G. *Macromolecules*, **1995**, *28*, 5267.
(29) Ruland, W. *Colloid Polym. Sci.* **1977**, *255*, 417.
(30) Magonov, S. *Polym. Mater. Sci. Eng.* **1998**, *78*, 106.
(31) Bar, G.; Thomann, Y.; Brandsch, R.; Cantow, H.-J. *Langmuir* **1997**, *13*, 3807.
(32) Microcal Origin 3.78, Microcal Software, Inc., Northampton, MA.
(33) In principle, the period should equal 1.986. This small difference, however, is within the error estimate. There is a small error because a sinusoidal function is only an approximate description of the true block like temperature profile. However, P_1 equals 1 when fitting the temperature profile with eq 10, as expected.
(34) Seiler, P. In *Accurate Molecular Structures: Their Determination and Importance*; Domenicano, A., Hargittai, I., Eds. Oxford University press: Oxford, England, 1992; Chapter 7.
(35) Swan, P. R. *J. Polym. Sci.* **1960**, *42*, 525.
(36) Hugel, T.; Strobl, G.; Thomann, R. *Acta Polym.* **1999**, *50*, 214.
(37) Magonov, S.; Godovsky, Y. *Am. Lab.* **1999**, April issue.
(38) Wunderlich, B. Crystal Structure, Morphology, Defects. In *Macromolecular Physics*; Academic Press: New York, 1973, Vol. 1.
(39) From a theoretical point of view the crystalline density relevant for SAXS does not have to be equal to that extracted from WAXD. The WAXD-based density is associated with that of the coherently scattering entities whereas the density relevant for SAXS is that of the entire lamella which can be lower due to defects of lower density at, e.g., grain boundaries.
(40) Barham, P. J.; Keller, A. *J. Polym. Sci. Part B: Polym. Phys.* **1989**, *27*, 1029.
(41) Albrecht, T.; Strobl, G. *Macromolecules* **1996**, *29*, 783.
(42) Blundell, D. J. *Polymer* **1978**, *19*, 1258.
(43) Strobl, G. R.; Schneider, M. *J. Polym. Sci., Polym. Phys. Ed.* **1980**, *18*, 1343.
(44) Vonk, C. G.; Pijpers, A. P. *J. Polym. Sci., Polym. Phys. Ed.* **1985**, *23*, 2517.

MA001759Y